

Proto-jets configurations in RADs orbiting a Kerr SMBH: symmetries and limiting surfaces

D. Pugliese & Z. Stuchlík

*Institute of Physics and Research Centre of Theoretical Physics and Astrophysics,
Faculty of Philosophy & Science, Bezručovo náměstí 13,
CZ-74601 Opava, Czech Republic*

(Dated: September 26, 2018)

Ringed accretion disks (**RADs**) are agglomerations of perfect-fluid tori orbiting around a single central attractor that could arise during complex matter inflows in active galactic nuclei. We focus our analysis to axisymmetric accretion tori orbiting in the equatorial plane of a supermassive Kerr black hole; equilibrium configurations, possible instabilities, and evolutionary sequences of **RADs** were discussed in our previous works. In the present work we discuss special instabilities related to open equipotential surfaces governing the material funnels emerging at various regions of the **RADs**, being located between two or more individual toroidal configurations of the agglomerate. These open structures could be associated to proto-jets. Boundary limiting surfaces are highlighted, connecting the emergency of the jet-like instabilities with the black hole dimensionless spin. These instabilities are observationally significant for active galactic nuclei, being related to outflows of matter in jets emerging from more than one torus of **RADs** orbiting around supermassive black holes.

Keywords: Black hole physics – jets – Gravitation – Hydrodynamics – Accretion, accretion disks – Galaxies: active – Galaxies: jets

I. INTRODUCTION

Spacetime symmetries play a dominant role in Astrophysics. The case of accretion disks, and especially the constrained axisymmetric (coplanar) tori orbiting a central Kerr supermassive black hole (**SMBH**) represents an example where both stable and unstable configurations can be predominantly determined by the geometric properties of the background.

More generally the physics of accretion disks is regulated by the balance of many factors influencing their evolution and morphology; magnetic fields, thermal or viscous processes for example play a combined and different role, from the phase of disk formation to accretion, eventually characterizing different accretion disk models. Nevertheless it is possible to trace a correlation between accretion disk models, determined by this special balance and the disk attractor itself. In the Polish-doughnut (P-D) thick accretion disk model [1], the role played by the curvature effects and spacetime symmetries is essential in setting constraints on axisymmetric accretion tori and in these situations, the geometric properties of the spacetime become relevant with respect to other ingredients in the determination of the disk forces balance. In here we consider ringed accretion disks (**RADs**), introduced in [2] and detailed in [3–6], featuring the formation and interaction of several, both corotating and counterrotating, axisymmetric (coplanar) tori orbiting a central Kerr **SMBH**.

These structures may form around **SMBH** in active galactic nuclei (**AGNs**), where the attractor, interacting with its environment during its life-time can give rise to different accretion periods. The case of a single orbiting torus stands as limiting case of the **RAD**.

The spacetime symmetries determined by the central attractor strongly constrain the configurations existence and stability. Properties of each torus are determined by an effective potential function enclosing the background Kerr geometry and the centrifugal effects. Equipotential surfaces, being

also equipressure surfaces, are associated with critical points identifying the toroidal surfaces of the disk. The cusped surfaces are the critical topologies associated to the torus unstable phases. The outflow of matter through the cusp occurs by the Paczynski mechanism of violation of mechanical equilibrium of the tori [7], i.e. an instability in the balance of the gravitational and inertial forces and the pressure gradients in the fluid [1]. The instabilities inside the ringed accretion disk may give rise to accretion into the attractor, whereas the open equipotential surfaces have been related to “proto jet-shell” structures, a general discussion of these special configurations can be found for example in [8–18]. The interaction between several launching points of jets, or other topologies of the decompositions, leads to collision in a couple, inducing a second instability phase with accretion or a further proto-jet formation, finally a phase, or a cycle, of a “drying-feeding” process between two **RADs** sub-configurations. In this work we concentrate our attention on these open configurations and their constraints.

From phenomenological viewpoint, the dynamics of the unstable phases of this system is significant for the high energy phenomena related to accretion onto super-massive black holes in **AGNs**, and the extremely energetic phenomena in quasars which could be observable in their X-ray emission, as the X-ray obscuration and absorption by one of the **RAD** ring. The radially oscillating tori of the ringed disk could be related to the high-frequency quasi periodic oscillations observed in non-thermal X-ray emission from compact objects (QPOs), a still obscure feature of the X-ray astronomy related to the inner parts of the disk. **BH** accretion rings models may be revealed by future X-ray spectroscopy, from the study of relatively indistinct excesses on top of the relativistically broadened spectral line profile [19–21]. The predicted relatively indistinct excesses of the relativistically broadened emission-line components, shall arise in a well-confined radial distance in the accretion disk, envisaging therefore a sort of rings model which may be adapted as a special case of the

model discussed in [3, 4].

In Section(II) we introduce the **RADs** model discussing the tori morphology, Sec. (II A) and Sec. (II B), while instabilities are considered in Section (III). Geometrical correlations of unstable configurations are discussed in Sec. (III A). Section (III B) is devoted to the parameter setting and discussion on the system rotational symmetries, in this section we provide also exact form of fluid specific angular momentum $\tilde{\ell}$ introduced in [4] and also considered in [6]. Analysis of the open configurations is in Section(IV), while in Section (IV A) restrictions on the existence of the open configurations are investigated introducing some limiting surfaces. Concluding remarks follow in Section (V).

II. TORI IN THE KERR SPACETIME

We start by presenting the Kerr metric tensor in the Boyer-Lindquist (BL) coordinates¹. $\{t, r, \theta, \phi\}$

$$ds^2 = -dt^2 + \frac{\rho^2}{\Delta} dr^2 + \rho^2 d\theta^2 + (r^2 + a^2) \sin^2 \theta d\phi^2 + \frac{2M}{\rho^2} r(dt - a \sin^2 \theta d\phi)^2, \quad (1)$$

$$\text{where } \rho^2 \equiv r^2 + a^2 \cos^2 \theta \quad \text{and} \quad \Delta \equiv r^2 - 2Mr + a^2,$$

$a = J/M \in [0, 1]$ is the specific angular momentum, M a mass parameter and J is the total angular momentum of the gravitational source. The non-rotating limiting case $a = 0$ is the Schwarzschild metric while the extreme Kerr black hole has dimensionless spin $a/M = 1$. Radii

$$r_h \equiv M + \sqrt{M^2 - a^2}; \quad r_c \equiv M - \sqrt{M^2 - a^2} \quad (2)$$

$$r_\epsilon^+ \equiv M + \sqrt{M^2 - a^2 \cos^2 \theta}; \quad (3)$$

are the horizons $r_c < r_h$ and the outer static limit r_ϵ^+ respectively, being $r_h < r_\epsilon^+$ on $\theta \neq 0$ and $r_\epsilon^+ = 2M$ in the equatorial plane $\theta = \pi/2$.

Ringed accretion disks are toroidal configurations of perfect fluids orbiting a central Kerr black hole (**BH**) attractor. Quantities

$$E \equiv -g_{\alpha\beta} \xi_t^\alpha p^\beta, \quad L \equiv g_{\alpha\beta} \xi_\phi^\alpha p^\beta, \quad (4)$$

are constants of motion, where the covariant components p_ϕ and p_t of a particle four-momentum are conserved along the geodesics. The constant L in Eq. (4) may be interpreted as the axial component of the angular momentum of a particle for timelike geodesics and E as representing the total energy of the test particle coming from radial infinity, as measured by a

static observer at infinity. This is a property derived from the presence of the two Killing vector fields $\xi_\phi = \partial_\phi$, rotational Killing field, and $\xi_t = \partial_t$, which is the Killing field representing the stationarity of the spacetime. In the test particle circular motion one can limit the analysis to the case of positive values of a for corotating ($L > 0$) and counterrotating ($L < 0$) orbits with respect to the black hole. In fact the metric tensor (1) is invariant under the application of any two different transformations: $x^\alpha \rightarrow -x^\alpha$ where $x^\alpha = (t, \phi)$, thus the metric is invariant for exchange of couple $(t, \phi) \rightarrow (-t, -\phi)$, or $(a, t) \rightarrow (-a, -t)$, or after a change $(a, \phi) \rightarrow (-a, -\phi)$, consequently, the test particle dynamics is invariant under the mutual transformation of the parameters $(a, L) \rightarrow (-a, -L)$.

It will be important to consider in the analysis of the ringed disks the notable radii $r_N^\pm \equiv \{r_\gamma^\pm, r_{mbo}^\pm, r_{mso}^\pm\}$, defining the geodesic structure of the Kerr spacetime with respect to the matter distribution. Specifically, for timelike particle orbits, r_γ^\pm is the *marginally circular orbit* or the photon circular orbit, timelike circular orbits can fill the spacetime region $r > r_\gamma^\pm$. The *marginally stable circular orbit* r_{mso}^\pm : stable orbits are in $r > r_{mso}^\pm$ for counterrotating and corotating particles respectively. The *marginally bounded circular orbit* is r_{mbo}^\pm , where $E_\pm(r_{mbo}^\pm) = 1$ [22–27]. The effective potential, regulating the motion of test particle circular geodesics can admit, as function of r/M , minimum points correspondent to particle stable circular orbits only in the region $r > r_{mso}^\pm$, respectively for counterrotating and corotating motion with respect to the central Kerr black hole; the effective potential admits the maximum points, correspondent to particle unstable circular orbits, only in the region $r \in]r_\gamma^\pm, r_{mso}^\pm[$. The energy E of the particle, as measured by an observer at infinity, will be greater than the value at infinity $E = \mu$, for the particle of mass μ on orbits in $r \in]r_\gamma^\pm, r_{mbo}^\pm[$, and the energy will be lower than limiting $E = \mu$, in the region $r \in]r_{mbo}^\pm, r_{mso}^\pm[$.

The geodesic structure represents a geometric property of the spacetime consisting of the union of the orbital regions with boundaries in r_N [4, 5, 28]. It can be decomposed, for $a \neq 0$, into the geodesic structures for corotating (r_N^-) and counterrotating (r_N^+) matter according to the convention adopted here and in [3]. Given $r_i \in r_N^\pm$, we adopt the notation for any function $\mathbf{Q}(r) : \mathbf{Q}_i \equiv \mathbf{Q}(r_i)$, therefore for example $\ell_{mso}^+ \equiv \ell_+(r_{mso}^+)$, and more generally given the radius r_* and the function $\mathbf{Q}(r)$, there is $\mathbf{Q}_* \equiv \mathbf{Q}(r_*)$.

For the symmetries of the problem, we assume $\partial_t \mathbf{Q} = 0$ and $\partial_\phi \mathbf{Q} = 0$, with \mathbf{Q} being a generic spacetime tensor [2, 29], and a one-species particle perfect fluid system described by the energy momentum tensor

$$T_{\alpha\beta} = (\varrho + p)u_\alpha u_\beta + p g_{\alpha\beta}, \quad (5)$$

where ϱ and p are the total energy density and pressure, respectively, as measured by an observer comoving with the fluid whose four-velocity u^α is a timelike flow vector field. *Continuity equation* and the *Euler equation* are respectively:

$$\begin{aligned} u^\alpha \nabla_\alpha \varrho + (p + \varrho) \nabla^\alpha u_\alpha &= 0 \\ (p + \varrho) u^\alpha \nabla_\alpha u^\gamma + h^{\beta\gamma} \nabla_\beta p &= 0 \\ h_{\alpha\beta} &= g_{\alpha\beta} + u_\alpha u_\beta, \quad (\nabla_\alpha g_{\beta\gamma} = 0) \end{aligned} \quad (6)$$

¹ We adopt the geometrical units $c = 1 = G$ and the $(-, +, +, +)$ signature, Greek indices run in $\{0, 1, 2, 3\}$. The four-velocity satisfy $u^\alpha u_\alpha = -1$. The radius r has unit of mass $[M]$, and the angular momentum units of $[M]^2$, the velocities $[u^t] = [u^r] = 1$ and $[u^\theta] = [u^\phi] = [M]^{-1}$ with $[u^\phi/u^t] = [M]^{-1}$ and $[u_\phi/u_t] = [M]$. For the seek of convenience, we always consider the dimensionless energy and effective potential $[V_{eff}] = 1$ and an angular momentum per unit of mass $[L]/[M] = [M]$.

We consider the fluid toroidal configurations (with $u^\theta = 0$) centered on the plane $\theta = \pi/2$, and defined by the constraint $u^r = 0$. Assuming a barotropic equation of state $p = p(\varrho)$, the Euler equation (6) provides the following equation

$$\frac{\partial_\mu p}{\varrho + p} = -\partial_\mu W + \frac{\Omega \partial_\mu \ell}{1 - \Omega \ell}, \quad \ell \equiv \frac{L}{E}, \quad W \equiv \ln V_{eff}(\ell) \quad (7)$$

$$V_{eff}(\ell) = u_t = \pm \sqrt{\frac{g_{\phi t}^2 - g_{tt} g_{\phi\phi}}{g_{\phi\phi} + 2\ell g_{\phi t} + \ell^2 g_{tt}}}, \quad \text{where on } \theta = \pi/2$$

$$V_{eff}^2(\ell) = \frac{\Delta \rho^2}{a^4 + a^2(\ell^2 + 2r^2) + r(r^3 - 4a\ell M) - \Delta(a^2 + \ell^2)} \quad (8)$$

(note that the effective potential $V_{eff}^2(\ell)$ is dimensionless). This potential is regulated by the radial profile of the geodesic specific angular momentum:

$$\ell = \frac{a^3 M + aMr(3r - 4M) \pm \sqrt{Mr^3 [a^2 + (r - 2M)r]^2}}{[Ma^2 - (r - 2M)^2 r]M} \quad (9)$$

while the continuity equation in Eq. (6) is identically satisfied as consequence of the applied conditions and symmetries. We note that Eq. (7) is a rearrangement of the Euler equation in Eq. (6). We singled out the variation of the specific angular momentum (ℓ) from the first term in r.h.s of Eq. (7), defining the effective potential and enclosing the information on the gravitational component of the torus forces balance. A relevant aspect of Eq. (7) is the shape of the toroidal configurations that can be found as the associated exact integrals. This is possible due to symmetries of the system and the assumption of a barotropic equation of state $p = p(\varrho)$. In this model, the fluid flow is not iso-entropic, the entropy S is not constant in space and time but it is constant along the fluid flow, i.e. $u^a \nabla_a S = 0$. In the V_{eff} definition, the normalization condition for the fluid four-velocity, $u^a u_a = -1$, has been taken into account, together with the definition of the parameterized specific angular momentum ℓ . Assuming $\ell = \text{constant}$, the second term of r.h.s of Eq. (7) vanishes. This special rewriting of the forces balance allows also identification of the critical points of the pressure. Both these aspects make the model extremely effective and versatile. On the other hand, there are several possible generalizations of this set-up: **1.** the first we mention here concerns the inclusion of other components in the balance of forces. The perfect fluid energy momentum tensor (5) can include for example a magnetic field component [30, 31]. **2.** secondly, we might consider the influence of the last term of Eq. (7) by adopting a varying fluid angular momentum $\ell(r)$ as, for example, in [32, 33].

Notice that we singled out definition of specific angular momentum of the fluid $\ell \equiv E/L$ in terms of the functions E and L , introduced in Eq. (4); these quantities are constants of motion for test particle circular orbits, according to the presence of the two Killing fields ξ_t and ξ_ϕ , and in the test particle scenario in the BL coordinate frame they have an immediate interpretation as quantities measured by a static observer at infinity. Nevertheless, for orbiting *extended* matter configurations, (E, L) are not (generally) constants of motion and an interpretation of these quantities has to be properly given.

Concerning the choice of $\ell = \text{constant}$, it is clear that in Eq. (5) we considered a simple fluid, i.e., made up by one species particles, which is subjected to pressure forces according to a barotropic equation of state. Other forces may have to be included as the magnetic or electric components in the energy momentum tensor. For the detailed discussion on relation between L , ℓ and E in the tori construction see for example [2].

We have therefore introduced the effective potential function $V_{eff}(\ell)$ for the fluid which reflects the contribution of the background Kerr geometry and the centrifugal effects. Ω is the relativistic angular frequency of the orbiting fluid relative to the distant observer. The specific angular momentum ℓ is considered here constant and conserved (see also [32, 34]).

As for the case of the test particle dynamics, due to the problem symmetries we can limit the analysis to positive values of $a > 0$, for *corotating* ($\ell > 0$) and *counterrotating* ($\ell < 0$) fluids and we adopt the notation (\pm) for counterrotating or corotating matter respectively (as $V_{eff}(\ell)$ in Eq. (7) is invariant under the mutual transformation of the parameters $(a, \ell) \rightarrow (-a, -\ell)$).

A. Ringed accretion disks

We consider a fully general relativistic model of ringed accretion disk (**RADs**) made by several corotating and counterrotating toroidal rings orbiting a supermassive Kerr attractor [3]. General Relativity hydrodynamic Boyer condition of equilibrium configurations of rotating perfect fluids governs the single torus. As a consequence of this many properties of the orbiting tori are determined by the effective potential. The toroidal surfaces are the equipotential surfaces of the effective potential (and equipressure surfaces) $V_{eff}(\ell)$, considered as function of r , solutions of $V_{eff} = K = \text{constant}$ or $\ln(V_{eff}) = c = \text{constant}$ [35]. These correspond also to the surfaces of constant density, specific angular momentum ℓ , and constant relativistic angular frequency Ω , where $\Omega = \Omega(\ell)$ as a consequence of the von Zeipel theorem² [30, 36].

Each Boyer surface turns to be identified by the couple of parameters (ℓ, K) .

B. RADs morphology

A torus in the **RAD** agglomerate can be corotating, $\ell a > 0$, or counterrotating, $\ell a < 0$, with respect to the central black hole rotation $a > 0$. Consequently, given a couple (C_a, C_b) with specific angular momentum (ℓ_a, ℓ_b) , orbiting in the equatorial plane of a central Kerr **SMBH**, we can introduce the concept of *lcorotating* tori, defined by the condition $\ell_a \ell_b > 0$, and *lcounterrotating* tori defined by the relations $\ell_a \ell_b < 0$. In

² More generally $\Sigma_{\mathbf{Q}}$ is the surface $\mathbf{Q} = \text{constant}$ for any quantity or set of quantities \mathbf{Q} . Therefore in this case $\Sigma_i = \text{constant}$ for $i \in (p, \rho, \ell, \Omega)$, where the angular frequency is indeed $\Omega = \Omega(\ell)$ and $\Sigma_i = \Sigma_j$ for $i, j \in (p, \rho, \ell, \Omega)$

other words, a couple of ℓ corotating tori can be both corotating $\ell a > 0$ or counterrotating $\ell a < 0$ with respect to the central attractor³ On the other hand, ℓ counterrotating couples are made of a corotating torus and a counterrotating torus, consequently the following two cases can occur: a couple can be composed by an inner corotating torus, with the respect to the **BH** and an outer counterrotating torus, or viceversa, the inner torus can be counterrotating and the outer one corotating.

Following this setup we focus on the solution of Eq. (7), $W = \text{constant}$, associated to the critical points, i.e., the extrema of the effective potential as functions of r/M , thus the minimum and maximum points of the effective potential, with angular momentum and parameter K in the ranges, $(\mathbf{K0}, \mathbf{L1})$ with $i = \{1, 2, 3\}$, and $(\mathbf{Kj}, \mathbf{L2})$, $j = \{0, 1\}$, represented in Fig. 2. In fact, only for K and ℓ parameters in these ranges, the effective potential function has extreme points. Specifically there are minima for $K \in \mathbf{K0}$ and $\ell \in \{\mathbf{L1}, \mathbf{L2}, \mathbf{L3}\}$, and there are maxima for $K \in \mathbf{K0}$ and $\ell \in \mathbf{L1}$, or $K \in \mathbf{K1}$ and $\ell \in \mathbf{L2}$. In Sec. (IV) we briefly discuss the solutions of $W = \text{constant}$ which are not associated to the extreme points of the effective potential, therefore we shall consider the other parameter regions of Fig. 2 –see for details [2].

Thus, more specifically we explore the orbital region $\Delta r_{crit} \equiv [r_{Max}, r_{min}]$, whose boundaries correspond to the maximum and minimum points of the effective potential respectively. The inner edge of the Boyer surface, the torus, must be at $r_{in} \in \Delta r_{crit}$, while the outer edge of the torus is at $r_{out} > r_{min}$. Then, there is a further matter configuration, which is closest to the central black hole and it is located at $r_{in} < r_{max}$. The limiting case of $K_{\pm} = K_{min}^{\pm}$ corresponds to a one-dimensional ring of matter located in r_{min}^{\pm} .

The centers, r_{cent} , of the closed configurations C_{\pm} , where the hydrostatic pressure is maximum, are located at the minimum points $r_{min} > r_{mso}^{\pm}$ of the effective potential. The toroidal surfaces are characterized by parameters $K_{\pm} \in [K_{min}^{\pm}, K_{Max}^{\pm}] \subset]K_{mso}^{\pm}, 1[\equiv \mathbf{K0}$ and specific angular momentum $\ell_{\pm} \leq \ell_{mso}^{\pm} \leq 0$ for counterrotating and corotating fluids respectively.

Therefore, the configurations have critical points, correspondent to the minimum and maximum of the hydrostatic pressure, more specifically then the maximum points of the effective potential r_{Max} correspond to minimum points of the hydrostatic pressure and the points of gravitational and hydrostatic instability. An accretion overflow of matter from the closed, cusped configurations in C_x^{\pm} (see Figs 3,4) can occur from the instability point $r_x^{\pm} \equiv r_{Max} \in]r_{mbo}^{\pm}, r_{mso}^{\pm}[$ towards the attractor, if $K_{Max} \in \mathbf{K0}^{\pm}$ with proper angular momentum $\ell \in]\ell_{mbo}^+, \ell_{mso}^+[\cup]\ell_{mso}^-, \ell_{mbo}^- [(\mathbf{L1}^+ \cup \mathbf{L1}^-)$, respectively, for counterrotating or corotating matter. Otherwise, there can be funnels of material, associated to matter jets, along an open configuration O_x^{\pm} having $K_{Max}^{\pm} \geq 1$ ($\mathbf{K1}^{\pm}$), launched from the point $r_j^{\pm} \equiv r_{Max} \in]r_{\gamma}^{\pm}, r_{mbo}^{\pm}[$ with proper angular momentum $\ell \in]\ell_{\gamma}^+, \ell_{mbo}^+[\cup]\ell_{mbo}^-, \ell_{\gamma}^- [(\mathbf{L2}^+ \cup \mathbf{L2}^-)$. We could refer to the

surfaces O_x^{\pm} as proto-jets, or for brevity jets⁴.

A second class of solutions are the equilibrium, not-accreting, closed configurations, with topology C , defining for $\pm \ell_{\mp} > \pm \ell_{mso}^{\mp}$ and centered in $r > r_{mso}^{\mp}$ respectively. However there are no maximum points of the effective potential for specific angular momentum $\pm \ell_{\mp} > \ell_{\gamma}^{\pm}$ ($\mathbf{L3}^{\mp}$), and therefore, only equilibrium configurations are possible for fluids having specific angular momenta in these ranges –see Figs 3,4.

To simplify our discussion in the following we use label (i) with $i \in \{1, 2, 3\}$ respectively, for any quantity \mathbf{Q} relative to the range of specific angular momentum \mathbf{Li} respectively, thus for example C_2^+ indicates a closed regular counterrotating configuration with specific angular momentum $\ell_2^+ \in \mathbf{L2}^+$. For the ordered sequences of surfaces in the **RADs**, with the notation $<$ or $>$, we intend the ordered sequence of maximum points of the pressure or r_{min} , minimum of the effective potential and the disk centers for the closed sub-configurations [4]. In relation to a couple of rings, the terms “internal” (equivalently inner) or “external” (equivalently outer), will always refer, unless otherwise specified, to the sequence ordered according to the location of the centers. Then, if $C_i < C_j$ for $i < j$, C_i is the inner ring, closest to attractor, with respect to C_j , and there is $r_{cent}^i \equiv r_{min}^i < r_{min}^j \equiv r_{cent}^j$. Within these definitions, the rings (C_i, C_{i+1}) and (C_{i-1}, C_i) are consecutive as $C_{i-1} < C_i < C_{i+1}$ [3]. The symbols $>$ and $<$ refer instead to the sequentiality between the ordered location of the minimum points of the pressure, or r_{Max} , maximum point of the effective potential, if they exist, which are the instability points of accretion, $r_x = r_{Max}$ for C_x topologies, or of launching of jets, $r_{Max} = r_j$ for the open cusped topologies (proto-jets). Therefore it is always

⁴ The role of “proto-jet” configurations, corresponding to limiting topologies for the closed or closed cusped solutions associated with equilibrium or accretion, is still under investigation. More generally, in this model the open surfaces with $\ell \in \mathbf{Li}$ have been always associated with the jet emission along the attractor symmetry axis—see for a general discussion [8–11, 14, 15, 18]. Although in Sec. (IV) we will briefly discuss the more general open configurations, in this work we mainly analyze the cusped open configurations considered as limiting surfaces associated with the two critical points of the effective potential, the inner one where the hydrostatic pressure is minimum, which is the instability point, and the outer one where the hydrostatic pressure is maximum, which is defined as “center” of the open configuration. The Boyer surfaces with sufficiently high specific angular momentum and elongation, i.e. $(\ell, K) \in \mathbf{L2} \times \mathbf{K1}$ (corresponding to centers which are far enough from the attractor, sufficiently high centrifugal component of the potential and sufficiently high density) are not capable to close forming an outer disk edge, but there is still a point of instability, r_j , at the inner edge. Since the nature of these configurations is a limiting evolutionary stage with respect to the other open topologies as well as to the equilibrium disk or closed disk in accretion, we referred to them shortly as proto-jet. It is clear that the problem to interpret these configurations invests the more general problem of the accretion-jet correlation which we also address in this work. In terms of proto-jet configurations ($\ell \in \mathbf{L2}$) it is necessary to investigate the relation between jets emission and accretion, particularly with respect to the location of the inner edge of the accreting disk (involving transition from the instability regions, for the parameter ranges $(\mathbf{L1}, \mathbf{L2})$), the magnitude of the disk specific angular momentum, and disk extension ($K \in \mathbf{K0}$ here also it linked to the size of the disk and its density and enthalpy). In this work, we attack the problem for the first time in framework of the ringed accretion disk, while a more accurate analysis of the interpretation of these open solutions, as well as of the emergence of other open configurations is left for further investigations.

³ In the following we will adopt often, when not required to do otherwise, the notation which does not explicit the fluid sign rotation. Then the discussion is intended to be independent from this and each ordering relation must be understood for each ℓ corotating sequence.

$r_{min}^i < r_{min}^o$. We note that only for an ℓ corotating sequence this definition implies also $r_{Max}^i > r_{Max}^o$. In other words, for the ℓ corotating sequences there is always $(\)_i < (\)_o$ and $(\)_i > (\)_o$, whereas for an ℓ counterrotating couple this is not always verified [4–6]. Here $(\)$ means any closed or open configuration.

As for the sequences of open configurations, O_x , we shall mainly deal with the relations between the critical points of the configurations, then it will be convenient to introduce the *criticality indices* \hat{i} , which are associated univocally to the couple (r_{Max}^i, ℓ_i) , where i is as usual the configuration index univocally associated to (r_{min}^i, ℓ_i) . We can note that $\hat{i}(i)$ is a decreasing function of the configuration index i (ordering the maximum of pressures) or $\partial_i \hat{i}(i) < 0$. Thus, for example, $O_x^i > O_x^o$ and $O_x^o > O_x^i$ where we have $|\ell_i| = |\ell_o| < |\ell_i| = |\ell_i|$.



FIG. 1. Pictorial representation of a ringed accretion disk with open O_x surfaces.

Finally, it should be noted that the simple case of barotropic tori with constant distribution of specific angular momentum provides all the relevant details of the **RAD** structure, as made up by thick toroidal disks, and at the present level of our knowledge it is a proper approximation to more realistic models. The effects on the adoption of more general laws for the fluid specific angular momentum in the tori model has been extensively discussed in the literature—see for example [32, 33]. Then, concerning the “piecewise” structure of the distribution of the ring specific angular momenta (the differential rotation of the ringed disk [3]), the rings are supposed to be formed in different accretion regimes and therefore it is natural (and necessary for the tori separation) that each torus is characterized by a different specific angular momentum.

III. RADS INSTABILITIES

The existence of a minimum of the hydrostatic pressure (r_{Max}) implies the existence of a critical topology for the fluid configuration—Figs 2,3,4. To sum up the situation for a **RAD** we may say there are two classes of points associated to the instability of the macro-structures: **1.** the Paczynski instability points (corresponding to violation of mechanical equilibrium

	$L0^\pm - K1^\pm$	$L1^\pm - K1^\pm$	$L2^\pm - K1^\pm$	$L3^\pm - K1^\pm$
	O_{in}^\pm	O_{in}^\pm	$O_x^{2\pm}$ O_{ext}^\pm	O_{ext}^\pm
1	$L0^\pm - K0^\pm$	$L1^\pm - K0^\pm$	$L2^\pm - K0^\pm$	$L3^\pm - K0^\pm$
	B_{in}^\pm	$(C_1^\pm, C_x^{1\pm})$ B_{in}^\pm	C_2^\pm	C_3^\pm
K_{mso}^\pm	$L0^\pm - K*^\pm$	$L1^\pm - K*^\pm$	$L2^\pm - K*^\pm$	$L3^\pm - K*^\pm$
	B_{in}^\pm	B_{in}^\pm	$[!B^\pm]$	$[!B^\pm]$
	$\mp \ell_{mso}^\pm$	$\mp \ell_{mbo}^\pm$	$\mp \ell_\gamma^\pm$	

FIG. 2. Scheme of the variation ranges $K \in \mathbf{Kj}$ where $j \in \{*, 0, 1\}$ and $\ell_i \in \mathbf{Li}$ where $i \in \{0, 1, 2, 3\}$ for the corotating (–) and counterrotating (+) cases respectively. K_{mso}^\pm is the value of the parameters K^\pm on the marginally stable orbit r_{mso}^\pm , while $\ell_{mso}^\pm \equiv \ell_\pm(r_{mso}^\pm)$, $\ell_\gamma^\pm \equiv \ell_\pm(r_\gamma^\pm)$, $\ell_{mbo}^\pm \equiv \ell_\pm(r_{mbo}^\pm)$ respectively. Radius r_γ^\pm is the photon orbit, and r_{mbo}^\pm is the marginally bounded orbit. White regions indicate the ranges $\mathbf{Li} - \mathbf{Kj}$ where critical points of the hydrostatic pressure are allowed. The topology of the Boyer surface is also indicated: C^\pm are the closed regular toroidal surface in equilibrium. C_x^\pm are the closed cusped surfaces with accretion point. O_x^\pm are open surfaces with a cusp (proto-jets) associated to the jet launch. The surfaces B^\pm and O^\pm are not associated to the critical points of the pressure. Sequences with B^\pm and O^\pm configurations for increasing K , with $\ell^\pm > \mp \ell_{mbo}^\pm$ constant are more articulated. In $\mathbf{L3} - \mathbf{Ki}$ no B surfaces appear ($[!B^\pm]$). In $\mathbf{L2} - \mathbf{Ki}$ the B surfaces are associated also with values $V_{eff} > 1$, thus these configuration could also be as B_{in} or B_{ext} kinds. Surfaces not associated to the critical points of the effective potential are discussed of Sec. (IV). –see Figs 3,4, a general discussion can be in Sec. (IV) and also [2]. The superscript, or equivalently subscript $\{\mathbf{Q}_i, \mathbf{Q}^i\}$ with $i \in \{1, 2, 3\}$ respectively, is for any quantity \mathbf{Q} relative to the range of specific angular momentum \mathbf{Li} .

in orbiting fluids see also [1, 37]), maxima of the effective potential $r_{Max} \in \{r_x, r_j\}$ for a O_x or a C_x topology and **2.** the contact points r_{\odot}^i (see [3]) between two surfaces of the decomposition featuring tori collision and associated to the second mode of instability for a \mathbf{C}_{\odot} ringed disk. Each ring may admit a maximum of two contact points r_{\odot}^i ⁵.

Consequently, we can identify two successive instability phases of the macro-configuration: the first (**I**) with the formation of one or more points of instability or involve two sub-configurations in the case of formation of a macro-configuration \mathbf{C}_{\odot} . (**II**) The second phase consists in the global instability of the ringed disk which follows the first phase. For both instability modes, in the second phase a penetration of matter from one unit to another is expected, and this can result in possible destabilization of the entire macro-structure by collisions between fluids. Then, although the second phase

⁵ The cusps (r_x, r_j) of the corotating surfaces can also occur in the spacetimes with $a > a_1$, while for spin $a = a_1 \equiv 1/\sqrt{2M} \approx 0.707107M$ the unstable point is on the static limit—see [28] and also [38] and Fig. 3. These surfaces are detailed in Sec. (IV).

in the two modes may be similar, the essential difference is in the first phase of instability which is, in the first mode induced by an instability point, while in the second mode, the presence of contact points is necessary. The Paczynski mechanism in the first mode may be involved as the cause of the second phase, while in the second mode, starting with a \mathbf{C}_\odot topology, of Paczynski instability could emerge in the second phase as a possible effect of the first phase of instability. In this work, we analyze the situation only in the first phase.

A. Geometrical correlations of unstable configurations

Concerning the possibility of collision and emergence of instability we introduce the concept of geometrical and causal correlation for unstable configurations of the **RAD**. Two sub-configurations of a ringed disk are said to be geometrically correlated if they are in contact, or they may be in contact according to some constraints settled on their morphological or topological evolution and the geodesic structure of the spacetime, i.e. according to the effective potentials they are subjected to [3]. We note that, since the intersection of the geodesic structures defined by r_N^\pm , and introduced in Sec. (II), is not empty, the analysis of the geodesic structure will be particularly important for the characterization of the geometrical correlation for the ℓ counterrotating sequences and particularly for the mixed subsequences. Thus part of this analysis is devoted to figure out whether and when two sub-configurations of a decomposition can be in contact, or, in fact, geometrically correlated according to a number of features set in advance, or which we seek to establish. A contact in this model causes collision and penetration of matter, eventually with the feeding of one sub-configuration with material and supply of specific angular momentum of another consecutive ring of the decomposition. This mechanism could possibly end in a change of the ring disk morphology and topology. In fact, several instability points can be geometrically correlated and present in a first phase of macro-structure instability, and being causally correlated, arising in a second phase of the macro-structure instability. The existence of a contact point in this model is governed by the geodesic structure of the Kerr geometry. It is clear that a geometrical correlation in a ringed structure induces a causal correlation in a couple, when the morphology or topology of an element can be regarded as a result of that correlation, which arises by the geometry of the common attractor⁶.

⁶ We note that the problem of inferring and even to define a causal correlation between events or objects can be indeed subtle and it is certainly relevant in a variety of scientific disciplines—for a very general discussion we refer to [39]. In the case of jet-proto-jet correlation and the jet-accretion correlation proposed here we should consider that generally correlation does not necessarily imply causation, and this latter aspect of the correlation should be faced more deeply together with a more general discussion of the correlation definition used here.

B. Parameter setting, rotational symmetry and $\check{\ell}$

In this section we investigate some symmetric properties of the angular momenta $\check{\ell} : V_{eff}(\check{\ell}, r) = 1$ introduced throughout the discussion of [4, 6], for a general radius r on the equatorial plane. This special specific angular momentum allows us to discuss some properties of symmetry of the effective potential inherited from the background symmetries and the toroidal motion of the orbiting system. An important role of the momentum $\check{\ell}$ has been widely studied as $\ell_{mbo} : V_{eff}(\ell_{mbo}, r_{mbo}) \equiv K_{mbo} = 1$ and $\partial_r V_{eff} = 0$ in $r = r_{mbo}$. Then clearly this is the asymptotic value of the effective potential for large r/M (or large $R = r/a$).

We can then reduce this problem to find out the solutions of the following equations

$$2\Delta_-^2 - (a^2 + \Delta_- \Delta_+) r + 2r^2 = 0 \quad \text{where} \quad (10)$$

$$V_{eff}(\Delta_\pm, r; a)^2 \equiv \frac{r\Delta}{2\Delta_-^2 - \Delta_- \Delta_+ r + r^3} > 0,$$

$$\Delta_\pm \equiv \ell \pm a, \quad \Delta_- \Delta_+ > 0, \quad \Delta_Q \geq 0 \quad \text{if} \quad \ell \geq 0, \quad (11)$$

$$\Delta_Q = \{\Delta_+, \Delta_-\}, \quad a > 0, \quad |\ell/a| > 1.$$

For sake of simplicity in this Section we mainly use dimensionless quantities where $r \rightarrow r/M$ and $a \rightarrow a/M$. Equation (10) is obtained by the condition $V_{eff}^2 - 1 = 0$ on the equatorial plane ($\theta = \pi/2$), while $V_{eff}(\Delta_\pm, r; a)^2$ is a rearrangement and a new parametrization of $V_{eff}(r; \ell, a)^2$ of Eq. (7) using new Δ_\pm . Note that $\Delta_\pm(-\ell) \leq 0$ for $\ell \geq 0$, and the quantity Δ_\pm in Eq. (10) should not be confused with Δ in the metric given by Eq. (1). No critical points exist, therefore, no Boyer surface exists, for $|\ell/a| < 1$ [2]. We will use Eq. (11), exploiting the symmetries in the couple Δ_\pm for sign reversal in the specific angular momentum. We have:

$$\ell = \frac{\Delta_- + \Delta_+}{2}, \quad a = \frac{(\Delta_+ - \Delta_-)}{2}, \quad (12)$$

$$V_{eff}(\Delta_\pm, r) \equiv \frac{1}{2} \sqrt{\frac{r[(\Delta_- - \Delta_+)^2 + 4(r-2)r]}{2\Delta_-^2 - \Delta_- \Delta_+ r + r^3}}.$$

Then we can introduce, a single rotation parameter for the system accretor-disk rather than two, defined by:

$$\mathcal{A}_\pm \equiv \frac{\Delta_\pm \mp \Delta_\mp}{2} : \quad \mathcal{A}_+ = a > 0, \quad \mathcal{A}_- = \ell, \quad (13)$$

where the two rotational parameters ℓ and a/M are now replaced by the two Δ_\pm .

The difference in the two forms of the potential in Eq. (10) and Eq. (12), respectively. This definition could be important in the analysis of accretion disks, because this reparametrization may result in the identification of significant traceable quantities, when the fluid specific angular momentum neither the attractor spin are not made explicit. Therefore, we expect these symmetries will be deepened further in a future work. Solving explicitly the problem (10) in terms of ℓ ,

one gets the two solutions

$$\check{\ell}_{\pm} \equiv \mp \frac{\pm 2a + \sqrt{2r\Delta}}{r-2}, \quad \check{\ell}_- < 0 \quad \forall r, \quad \check{\ell}_+ < 0 \quad \text{in } r < r_{\epsilon}^+,$$

where $\check{\ell}_{\pm} = \check{\ell}_{\pm}(r_{mso}^{\pm})$ $\check{\ell}_{2+}^- = \check{\ell}_+(r_{mso}^-)$. (14)

Therefore, the specific angular momentum $\check{\ell}$ is provided by Eq. (14) and, considered the form of the radii r_{mso}^{\pm} , the symmetries between of the ℓ counterrotating fluid configurations at the marginally stable orbits are clear. However, we can investigate more deeply this aspect, using the variables Δ_{\pm} . Then the solutions (10) are the couples:

$$(\Delta_-^{[-]}, \Delta_+^{[+]}) \quad \text{and} \quad (\Delta_-^{[+]}, \Delta_+^{[-]}) \quad \text{where} \quad (15)$$

$$\Delta_{\pm}^{[\pm]} \equiv -\frac{ar \pm \sqrt{2}\sqrt{r\Delta}}{r-2}, \quad \Delta_{\pm}^{[\pm]} = \frac{a(r-4) \pm \sqrt{2}\sqrt{r\Delta}}{r-2}.$$

Considering the following symmetries:

$$\Delta_+(\ell) = -\Delta_-(-\ell), \quad \Delta_+(-\ell) = -\Delta_-(\ell) \quad (16)$$

$$\Delta_-(-\ell)^2 = \Delta_+(\ell)^2, \quad \Delta_-(\ell)^2 = \Delta_+(-\ell)^2, \quad (17)$$

$$\Delta_+(\ell)\Delta_-(\ell) = \Delta_-(-\ell)\Delta_+(-\ell)$$

and having in mind also Eq. (11), we can say that a change in sign $-1\Delta_{\mathbf{Q}}$ acts in exchanging the subscript sign Δ_{\pm} and ℓ . Then we can solve the Boyer problem to find out the ring surfaces in terms of the resolving couples Δ_{\pm} . By considering effective potential $V_{eff}(\Delta_{\pm}, r)^2$ in Eq. (10), we get the following solutions for the specific angular momenta of the critical points for the pressures where solutions of the Boyer problem exist:

$$\Delta_- = \frac{a(r-1)r^2 - \sqrt{r^3\Delta^2}}{\Delta + X}, \quad \text{and} \quad (18)$$

$$\Delta_+ = -\frac{-\{2a^3 - ar[8 + (r-7)r]\} + \sqrt{r^3\Delta^2}}{\Delta + X},$$

$$\Delta_- = \frac{a(r-1)r^2 + \sqrt{r^3\Delta^2}}{\Delta + X} \quad \text{and} \quad (19)$$

$$\Delta_+ = \frac{2a^3 - ar[8 + r(r-7)] + \sqrt{r^3\Delta^2}}{\Delta + X}, \quad X \equiv -r(r-2)(r-1).$$

where $\Delta_+ - \Delta_- = 2a$. Similar considerations are also possible considering the situation on different planes, for example by considering the quantity $\ell/a \sin \theta$, see for example [2], and possibly generalizing the specific angular momentum definition [32].

However, it is convenient to take advantage of the symmetries of the configuration in the treatment of extended systems of matter in the axisymmetric fields, and particularly the symmetry of reflection on the equatorial plane. In the re-parametrization $(\ell, a/M) \mapsto \Delta_{\pm}$ we can take advantage of the symmetries in Eq. (16), managing only one sign, then reducing to *one only, always positive* variable Δ_+ or Δ_- , without considering the corotation or counterrotation nature of the fluid (that could indeed be difficult to be assessed) but considering Eq. (17). The square Δ_{\pm}^2 is the only term of the potential in Eq. (10) that changes subscript after a change of the specific angular momentum. Suppose for simplicity $\ell > 0$, then, being

Δ_{\pm} , the variable, we can solve for one of the two Δ_{\pm} and then use any of the symmetries in Eq. (16) to infer information on the other one.

IV. OPEN EQUIPOTENTIAL SURFACES AND FLUID CONFIGURATIONS

The existence of the fluid configurations is schematically summarized in Fig. 2 in terms on the ranges of the specific angular momentum and the K parameter.

In [4] we discussed the configurations associated with the pressure critical points, occurring for the parameter ranges $\mathbf{Li} \cup \mathbf{Kj}$, with $\mathbf{Ki} \in \{\mathbf{K0}, \mathbf{K1}\}$, and $\mathbf{Li} \in \{\mathbf{L1}, \mathbf{L2}\}$, or $\mathbf{L3} \cup \mathbf{K0}$. Here, we add some comments on the surfaces not associated to the critical points of the effective potential function but the solutions of $V_{eff}(\ell, r) = K$. In the following, we address the discussion in terms of the specific angular momentum magnitude unless the fluid rotation with respect to the black hole is not explicitly specified.

We start our considerations by noting that the hydrostatic pressure has a monotonic behavior as a function of r/M for specific angular momentum in $\mathbf{L0}$: $\ell < \ell_{mso}$, where $V_{eff} < 1$ on the equatorial plane. For these values of specific angular momentum ℓ , there are no critical points of the fluid pressure. As proved in [2], the case $\bar{\ell} \equiv |\ell/a| < 1$ is a restriction of $\mathbf{L0}$ on the equatorial plane⁷. At $K < 1$, range $\mathbf{K0}$, and $\ell < \ell_{mso}$, range $\mathbf{L0}$, no critical points of the effective potential occur on the equatorial plane: the pressure generally decreases with the radius (on the plane Σ_{ϵ}^+). However, at $\mathbf{L0} \cup \mathbf{K0}$ there are the \mathbf{B}_{in} surfaces, fat closed tori as shown in Fig. 4. Funnels are not associated to these solutions. The unique solution of the problem $V_{eff} = K < 1$ corresponds to the outer edge of this configurations. The surface becomes smaller for decreasing $K \in \mathbf{K0}$. The surface area increases by decreasing the specific angular momentum magnitude $\ell \in \mathbf{L0}$. Qualitatively we could conclude that the rotation relative to the attractor plays an irrelevant role in the determination of the morphology of these surfaces, which confirms a symmetry between the ℓ counterrotating sequences as pointed out in [2] and [3]. However, these features distinguish morphologically the \mathbf{B}_{in} from the lobe \mathbf{B}_{ext} which appears at higher specific angular momenta. Decreasing the specific angular momentum from starting value $\ell \in \mathbf{L3}$, when there is a maximum of the hydrostatic pressure, a first surface B_{ext} occurs. At $K \geq K_{min}$, a toroidal ring is formed, this grows and approaches the attractor as the specific angular momentum magnitude decreases. If $K_{Max} < 1$, i.e. $\ell \in \mathbf{L1}$, then with decreasing of the specific angular momentum in $\mathbf{L1}$ towards values in $\mathbf{L0}$, a B_{in} inner surface appears (i.e. one has the sequence of configurations $\{\mathbf{B}_{ext}, \mathbf{C}, \mathbf{C}_x, \mathbf{B}_{in}\}$), with no open funnel—Fig. 4.

For $K \geq 1$, open surfaces of funnels of matter appear, close to the rotation axis as the specific angular momentum mag-

⁷ On the planes different from the equatorial one, we can generalize the limit by assuming $\bar{\ell} \equiv \ell/a\sigma < 1$ $]-1, 1[$ or, as discussed below, $\bar{\ell} \equiv \ell/a\sigma \in]-1, 1[$, with $\sigma = \sin \theta$, where no critical points are possible—see also [2].

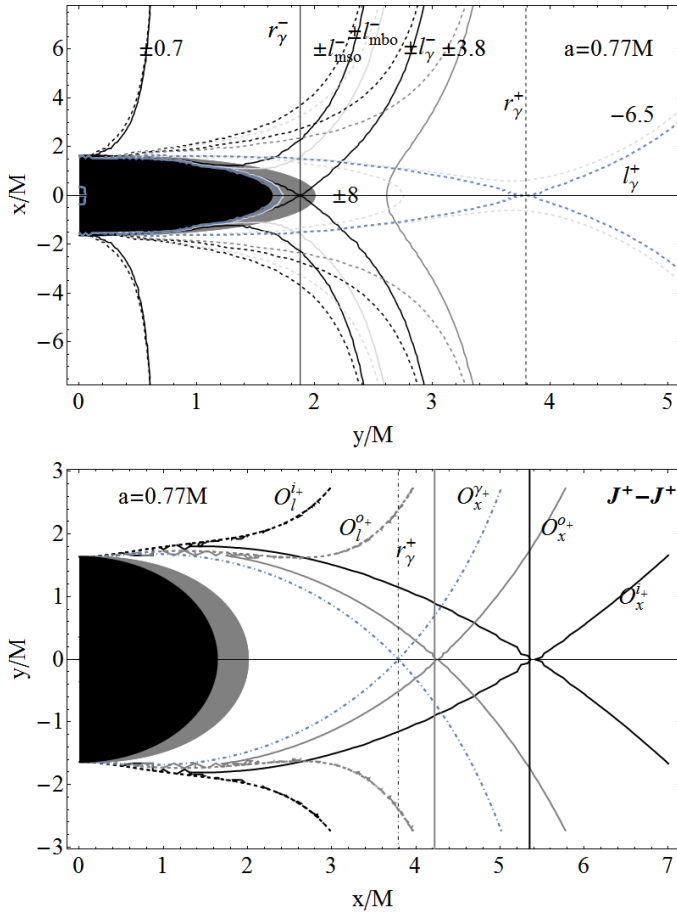


FIG. 3. *Upper*: Spacetime spin $a = 0.77M$, ℓ counterrotating sequences, $\ell_i \ell_j < 0$. The outer horizon is at $r_h = 1.63804M$, the region $r < r_h$ is black-colored, the region $r < r_\epsilon^+$ is gray colored, radius r_ϵ^+ marks the static limit. Surfaces in the $x - y$ plane, for different values of specific angular momentum ℓ for corotating ($\ell > 0$ -continuum lines) and counterrotating ($\ell < 0$ -dashed lines) fluids. r_γ^\pm are the photon circular orbits were $\ell_{mso} = \ell(r_{mso})$ and $\ell_\gamma = \ell(r_\gamma)$. Radius r_{mso} is the marginally stable orbit. The superscript (\pm) is for corotating ($-$) and counterrotating ($+$) matter respectively. The numbers close to the curve are the values of the specific angular momentum [4]. *Below*: spacetime spin $a = 0.77M$, ℓ corotating sequences, $\ell_i \ell_j > 0$, of counterrotating open configurations $\mathbf{J}^+ - \mathbf{J}^+$, $a < 0 \forall ij$. Decomposition including open-crossed sub-configurations (γ -surface) O_x^\pm , open cusped with angular momentum ℓ_γ . The outer horizon is at $r_h = 1.63804M$, black region is $r < r_h$, gray region is $r < r_\epsilon^+$, where r_ϵ^+ is the static limit, and r_γ^+ is the photon orbit on $\Sigma_{\pi/2}$. For O_x^\pm there is $\ell_o = -5.62551$ and $K_o = 1.28775$, for O_x^\pm there is $\ell_i = -4.66487$ and $K_i = 1.00272$. The hy -surfaces, O_i^\pm and O_j^\pm are also plotted—see also Sec. (IV)

nitude decreases in $\ell \in \mathbf{L0}$. These configurations will be referred as O_{in} . This surfaces (where $\partial_x y > 0$) do not cross the axes $y = 0$ —see Fig. 4⁸

⁸ Increasing $K \in \mathbf{K1}$, or decreasing $|\ell| \in \mathbf{L0}$ a collimation occurs, i.e., there

A. Restrictions on the existence of the open configurations: limiting surfaces

The set of O and B_{ext} configurations which are not related to the critical points of the effective potential correspond to the solutions $\Pi = 0$ of:

$$\Pi(\ell) = g_{\phi\phi} + 2\ell g_{\phi t} + \ell^2 g_{tt}, \quad (20)$$

— see Figs 3,4. The effective potential, related to the four-velocity component $u_t = g_{\phi t} u^\phi + g_{tt} u^t$, is not well defined on the zeros of $\Pi(\ell)$.

Decomposing explicitly the function ℓ in terms of the quantities $\Sigma = u^t$ and $\Phi = u^\phi$ then, the quantity Π can be written as $\Pi(\Sigma, \Phi) = g_{tt}(\Sigma)^2 + 2g_{\phi t}\Sigma\Phi + g_{\phi\phi}\Phi^2$. Thus, Π is related to the normalization factor γ for the stationary observers, establishing thereby the light-surfaces (for example [40, 41]). Alternatively, by expressing the effective potential in terms of $L(\ell)$, and by using definition Eq. (4) and definition of ℓ in Eq. (7), one obtains $\Pi(L, E) = E^2 g_{\phi\phi} + 2E g_{\phi t} L(\ell) + g_{tt} L(\ell)^2$.

The attractor-ringed-disk system shows various symmetry properties with respect to the rationalization $\bar{\ell} = \ell/(a\sigma)$ and $R = r/a$, where $\sigma = \sin \theta$ [2]. These quantities are dimensionless and, assuming $a > 0$ with ℓ positive or negative according to the fluids rotation, the parameter $\bar{\ell}$, takes care of the symmetry for reflection on the equatorial plane through σ . No-

would be $\partial_{|x|}|y|_x < 0$ but $\partial_{|x|}|y|_{|x|} > 0$. As in [6], we can define collimation of the funnels along the rotation axis if there is at least one $x_c : \partial_{|x|}|y| < 0$ for $x > x_c$ where the rotation axis is located at $y = 0$. The open surface will be said collimated, the coordinate x_c , and the corresponding y_c , give the collimation points. If $\partial_{|x|}|y| = 0$, in a given finite region of x , then the funnel structure is tubular, formed by matter rotating around the x axis at each Σ_t (in this model $\dot{r} = 0$). In the tubular structure the radius of the cylinder remains constant for each y . In the proto-jets there should be some mechanism pushing the matter to induce a $\partial_{|x|}|y| < 0$ by changing also accordingly the specific angular momentum magnitude or K parameter. For example, one might ask if a change of spin of the attractor could constitute such a factor, or also one can equally consider the case of the open critical configurations O_x . For a general discussion on the role of the open surfaces and their connection with jet emission we refer to [8–11, 14, 15, 18]. Then, given an ℓ corotating $O_x^i < O_x^j$ couple, it is always $O_x^i > O_x^j$ at $r < r_j^i$ and $O_x^i < O_x^j$ for $r > r_j^i$, and there is a couple of cross points ($O_x^i \cap O_x^j \neq \emptyset$) in $]r_j^i, r_j^j[$ —see Fig. 3. This means that, given $\bar{x} < r_j^i$ on the equatorial plane, there is $|O_x^i| \equiv |\bar{y}^i| > |O_x^j| \equiv |\bar{y}^j|$. In other words, the curve O_x^i is contained in the region of the $y - x$ plane with boundary O_x^j for $r < r_j^i$. Viceversa, at $r > r_j^i$ the (open) surface O_x^i is contained in the region of the plane cut by O_x^j , or for $\bar{x} > r_j^i$ on the equatorial plane, there is $|O_x^i| \equiv |\bar{y}^i| < |O_x^j| \equiv |\bar{y}^j|$. This means, in particular, that the funnels of ℓ corotating couple of open surfaces do not cross each other in the region $r > r_j^i$ and generally the separation $|\bar{y}^j| - |\bar{y}^i|$ increases with $r > r_j^i$. But they approach to the axis in the region close to the instability launch point r_j , and for higher specific angular momentum $|\ell|$. Though, in this model of axisymmetric fluids with constant specific angular momentum, there is no “collimation” of the funnels or, if $x=0$ is the rotation axis, it is $\partial_{|y|}|\bar{x}| > 0$ on the equatorial plane, where $|\bar{x}| > r_j$. Nevertheless any matter in open funnels, with specific angular momentum in $|\ell^i, \ell^o|$, will be bounded by the couple of configurations $O_x^i < O_x^o$. Then $\partial_x(y_\delta - y_i) > 0$ (on the section $x > 0$ and $y > 0$), the minimum value of the distance $(y_\delta - y_i)$ is reached in the equatorial plane, where $x = 0$.

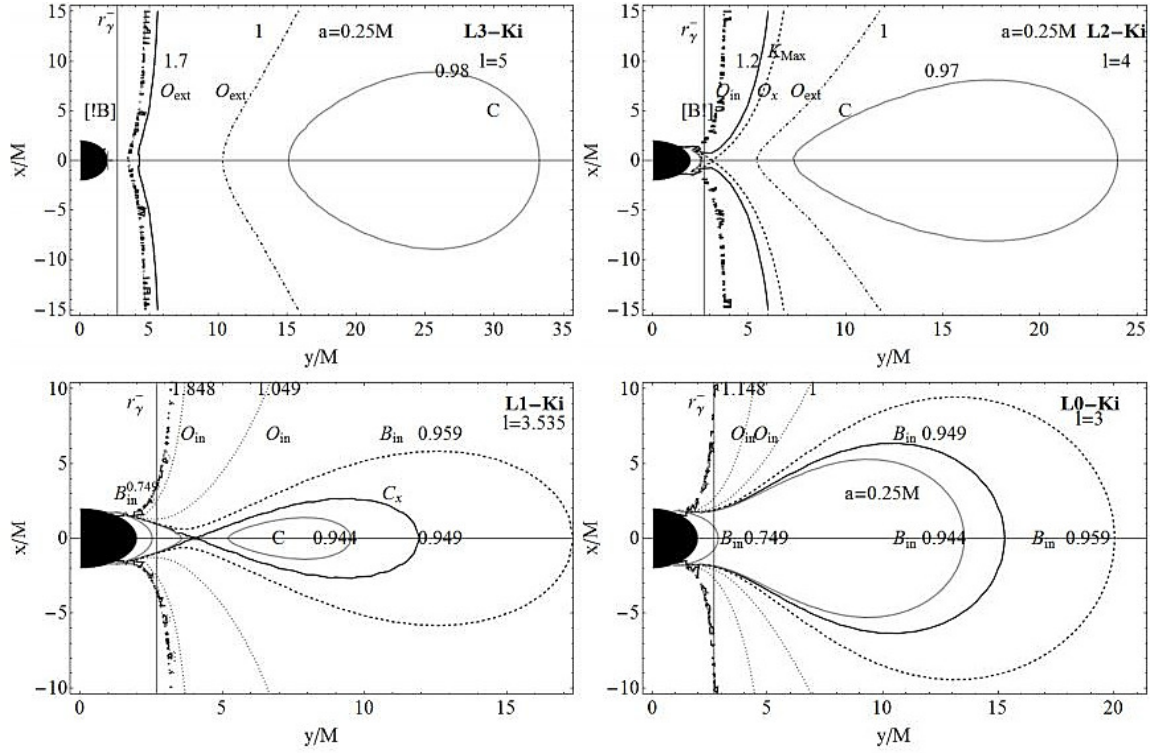


FIG. 4. Spacetime spin $a = 0.25M$, ℓ corotating sequences, $\ell_i \ell_j > 0$, of corotating disks $\ell_i a > 0 \forall ij$. Decompositions including open-crossed sub-configurations O_x . The outer horizon is at $r_h = 1.96825M$, the region $r < r_h$ is black-colored. In **L3 – Ki** no B surfaces appear ([!B]). Surfaces not associated to the critical points of the effective potential are discussed of Sec. (IV).

ticeably, many properties of the **RAD** depend mainly on the rationalized specific angular momentum $\bar{\ell}$. We discuss this kind of symmetry in Sec. (III B). To characterize the dependence on a , and the **RAD** symmetry properties with respect to the equatorial plane, it is convenient to rewrite the quantity Π in terms of $\bar{\ell}$ and $\bar{\ell} \equiv \bar{\ell}/\sigma$ as follows

$$\Pi(\bar{\ell}, R) = -a^3 \sigma^2 \left[2(\bar{\ell} - 1)^2 R \sigma^2 + a(1 + R^2 - \sigma^2)(1 + R^2 - \bar{\ell}^2 \sigma^2) \right]$$

$$\Pi(\bar{\ell}, R) = -a^3 \sigma^2 \left[2(\bar{\ell} - \sigma)^2 R + a(1 + R^2 - \sigma^2)(1 + R^2 - \bar{\ell}^2) \right], \quad (2b)$$

in dimensionless quantities. At fixed specific angular momentum ℓ , the zeros of the Π function define *limiting surfaces* of the fluid configurations—Figs 3,4. For fluids with specific angular momentum $\ell \in \mathbf{L3}$, the limiting surfaces are the cylinder-like surfaces O_{ext} , crossing the equatorial plane on a point which is increasingly far from the attractor with increasing specific angular momentum magnitude. A second B -like surface, embracing the **BH**, appears, matching the outer surface at the cusp r_γ . Decreasing the specific angular momentum magnitude ℓ towards the limiting value ℓ_γ , the surface $y(x)$, symmetric with respect to the equatorial plane, has a minimum at $x = 0$ —Eq. (21). Then, for $\ell = \ell_\gamma$ a cusp appears together with a inner surface closed on the **BH**.

The morphology of these surfaces is analogue to the matter funnels of the open topologies having $\ell \in \mathbf{L2}$ and $K \in \mathbf{K1}$. In this sense, the light-surfaces, for $\ell = \ell_\gamma$, can be interpreted as “limiting surfaces” of the open Boyer surfaces. Decreasing the specific angular momentum ℓ , from a starting $\ell \in \mathbf{L3}$, the O_{ext} surfaces open up at the radius r_γ in $r < r_\gamma$, and approaching the horizon as a O_{in} topology towards the rotation axes as shown in Figs 3,4. Comparing with the corotating surfaces, because of their rotation with respect to the black hole, the light-surfaces for the counterrotating fluids form in more distant orbital regions. This fact implies the emergence of a broad diversification of the unstable rotating structures for these fluids—see Fig. 3.

More generally, we can introduce the limiting geometric surfaces, or γ -surfaces, related to the geometric properties of the Kerr spacetimes, formed by the surfaces given by the solution of Eq. (7) and associated to the specific angular momentum $\{\ell_{mso}^\pm, \ell_{mbo}^\pm, \ell_\gamma^\pm\}_{\pi/2}$.

On the other hand, the solutions of $\Pi(\ell) = 0$, for fixed parameters ℓ and a/M , define the limiting hydrostatic surfaces, hy -surfaces, (with the notation $()^\ell$), which are associated with each hypersurface Σ_ℓ , whose topology and morphology changes with the variation of one of the two rotational parameters $(\ell, a/M)$. More specifically, the hy -surfaces are the limiting surfaces to which the fluid configuration belonging to the same topological class, and determined by the Euler problem on $\Sigma_\ell \cup \Sigma_a$, approaches, at the variation of the free K -parameter. The γ -surfaces, on the other hand, constraint the fluid at variation of ℓ . At $\Sigma_{a/M}$, the γ -surfaces are the limits of the hy -surfaces, approached by varying ℓ ; the hy -surfaces in turn limit the matter fluid surfaces as described below. In Fig. 3 an example of an ℓ corotating sequence of counterrotating hy -surfaces, the inner one O_i^{t+} and outer O_i^{o+} one, is shown.

The γ -surfaces define, for the ℓ counterrotating sequences on a $\Sigma_{a/M}$, three geometric regions depending on the attrac-

tor spin: **1.** an external region, or $r > r_\gamma^+$, confined by the γ -surface $O_x^{\gamma+}$ associated to the counterrotating photon-orbit with a cusp at r_γ^+ . **2.** the region in $]r_\gamma^-, r_\gamma^+[$, and finally **3.** an internal region at $]r_h, r_\gamma^-]$. The open γ -surface $O_x^{\gamma-}$ is cusped in r_γ^- , and it corresponds to the corotating photon orbit, see Fig. 3. The two critical surfaces $O_x^{\gamma\pm}$, have one lobe closed on the black hole and the location on the corotating closed lobe of $O_x^{\gamma-}$ is *inside* the $O_x^{\gamma+}$ configuration and, for $2b < a_1 = 0.707107M$ this is inside the ergoregion of the Kerr spacetime, see [28].

Since there is $\ell_{mbo} \in]\ell_{mso}, \ell_\gamma[$, the γ -surfaces associated to the specific angular momenta ℓ_{mso} and ℓ_{mbo} , belong to the internal region, and thus they are configurations of the O_{in}^γ type—see Figs 1,2,3,4. There are no γ -surfaces in the external region. For the specific angular momentum ℓ_i on each hyperplane $\Sigma_{a/M}$, these surfaces are in turn determined a priori on each $\Sigma_{a/M}$, whatever the specific angular momentum ℓ of the fluid is on that plane. The hy -surfaces have a cusped topology on the equatorial plane at r_γ^\pm for counterrotating and corotating fluids respectively. We note that the investigation of these regions is useful in particular for the analysis of the ℓ counterrotating sequences at each Σ_a . In fact, the limiting hydrostatic surfaces are never cusped but at $\ell = \ell_\gamma$, where we have the topological class O_x^ℓ , which coincide with the geometric light surfaces, or $O_x^\ell \equiv O_x^\ell$, closed on the black hole and opened outwards. For the specific angular momentum $\ell = \ell_\gamma^\pm$, the matter configurations, limited by $O_x^\ell \equiv O_x^\ell$, can be closed, centered in $r_c > r_{mso}$ for $K \in \mathbf{K0}$, or can be open in $O_{ext} > O_x^\ell$ for $K \in \mathbf{K1}$. The surface O_x^ℓ is a boundary surface reached by lowering the specific angular momentum towards ℓ_γ , or

$$\lim_{|\ell| \rightarrow |\ell_\gamma|} O_{ext} \approx O_x^\ell, \quad r_{ext} > r_\gamma, \quad O_{ext} > O_x^\ell, \quad |\ell_{ext}| > |\ell_\gamma|, \quad (22)$$

where r_{ext} is the crossing point of O on the equatorial plane⁹. This is not a cusp but it is a regular, minimum point of the curve $y(x)$. Therefore, the matter surfaces O_{ext} have a critical point of the hydrostatic pressure, a maximum in r_x but, like the correspondent hy -surface O_{ext}^ℓ , it is open and regular.

Concluding, there are three classes of open matter configurations, $O_i \in \{O_x, O_{in}, O_{ext}\}$, bounded by the limiting hydrostatic surfaces $O_i^\ell \in \{O_x^\ell, O_{in}^\ell, O_{ext}^\ell\}$ respectively, where $O_x^\ell \equiv O_x^\ell$. Each class of limiting surface O_i^ℓ is bounded by the correspondent open hy -surface, O_i^γ , and it approaches O_i^γ varying K . Therefore the two classes O_{ext}^ℓ and O_{in}^ℓ of open surfaces are separated by $O_x^\ell = O_x^\ell$, so that there is

$$O_{in}^{\ell_{in}} < O_{in}(\ell_{in}) < O_x^\ell = O_x^\ell < O_{ext}^{\ell_{ext}} < O_{ext}(\ell_{ext}), \quad (23)$$

$$\text{with } \ell_{in} < \ell_\gamma < \ell_{ext} \text{ and}$$

$$O_x^\ell = O_x^\ell < O_x(\bar{\ell}) < O_{ext}^{\ell_{ext}} < O_{ext}(\ell_{ext}) \quad (24)$$

$$\text{with } \bar{\ell} < \ell_{in} < \ell_\gamma < \ell_{ext}.$$

⁹ In these cases the sequentiality will be intended according to the ordered sequences of the equatorial crosses r_{ext} for the open, not-cusped, O_{ext} surfaces.

On the other hand, there are the limiting specific angular momenta at $\ell_{mbo} > \ell_{mso}$, leading both to O_{in}^γ : or $O_{in}^\ell(\ell_{mbo}) = O_{in}^\gamma(\ell_{mbo}) > O_{in}^\gamma(\ell_{mso}) = O_{in}^\ell(\ell_{mso})$.

The matter surfaces O_x are bounded by the limiting O_x^γ , solution of $\Pi = 0$. The matter surfaces $O_{ext} > O_x^\gamma$ and $O_{in} < O_x^\gamma$ are bounded by O_x^γ , with specific angular momentum fixed in ℓ_γ . They are also bounded by the solutions of $\Pi(\ell) = 0$, for the same specific angular momentum, and having equal topology $O_{ext} > O_{ext}^\ell > O_x^\gamma$. The γ -surfaces are approached by changing the specific angular momentum (see Eq. (23)). While the hy -surfaces are generally approached by an asymptotic limit of K , as it is clear from Fig. 2.

We note that the second and third inequality in Eq. (23) (and the first and second of Eq. (24)) are ensured by the relations among the specific angular momentum of the ℓ corotating sequences, as the following general relations hold

$$\partial_{\mathbf{Q}} r_{crit}^{[\mp]} \leq 0, \quad r_{crit}^{[+]} = r_{min} = r_{cent}, \quad (25)$$

$$r_{crit}^{[-]} \in \{r_{Max} = r_x, r_{Max} = r_J, r_{int}, r_{ext}\}, \quad \mathbf{Q} \in \{|\ell|, K\}, (26)$$

in particular for $\mathbf{Q} = |\ell|$, where Eq. (25), for $\mathbf{Q} = |\ell|$, does not apply to the first and last inclusion relations of Eq. (23) because the two couples of open surfaces (O_{ext}, O_{ext}^ℓ) and (O_{in}, O_{in}^ℓ), respectively, have the same topology and the same specific angular momentum, the limit indeed is approached changing the K parameter or for $\mathbf{Q} = K$. Thus, the non-cusped limiting surfaces can be the regular couples $B_{ext}^\ell < O_{ext}^\ell$, when $\ell \in \mathbf{L3}$, that is $\ell > \ell_\gamma$, in the external region, according to Figs 2,3,4.

Associated with these configurations, there is the couple $B_{ext} < O_{ext}$ in $\mathbf{L3} \cup \mathbf{K1}$. Otherwise there can be, in the internal region, also a O_{in}^γ surface for specific angular momentum $\ell < \ell_\gamma$ embracing the horizon. The O_{in} surfaces are due to the cusp opening occurring when the magnitude of the specific angular momentum decreases (where $\partial_{y^2}^2 x > 0$). There are therefore the hy -surfaces O_{in}^ℓ , approaching the proper limits on the specific angular momentum (starting by initial data in $\mathbf{L0}$, $\mathbf{L1}$ or $\mathbf{L2}$) the γ -surfaces O_{in}^γ , zeros of Eq. (20) for $\ell = \{\ell_{mso}, \ell_{mbo}\}$. Indeed, decreasing $\ell_0 \in \mathbf{L3}$, we have the hy -surfaces sequences: $\{(B_{ext}^\gamma < O_{ext}^\gamma)|_{\mathbf{L3}}, O_x^\gamma|_{\ell_\gamma}, O_{in}^\gamma|_{\ell < \ell_\gamma}\}$. For the open crossed surfaces O_x (for $\ell \in \mathbf{L2}$) there are

$$\lim_{\ell \rightarrow \ell_\gamma} O_x \approx O_x^\gamma = O_x^\ell, \quad O_x > O_x^\gamma \quad r_x = r_J > r_x^\gamma, \quad O_x < O_x^\gamma, \quad (27)$$

see also Eq. (22) and Fig. 3. The open surfaces O_{ext} are limited by the configurations O_{ext}^γ , in other words $r_{ext} = y_3 > r_{ext}^\gamma$, where $O_{ext} > O_{ext}^\gamma$ —Fig. 3. There is also $B_{ext}^\gamma < O_{ext}^\gamma$, and $\partial_{|\ell \in \mathbf{L3}|} B_{ext}^\gamma > 0$, $\partial_{|\ell \in \mathbf{L3}|} r_{ext}^\gamma > 0$. For specific angular momentum $\ell < \ell_\gamma$, there are the open surfaces ($O_{in}^\gamma, O_{in}^\ell, O_{in}$). Whereas, for $\ell \in \mathbf{L2}$, there are the surfaces $\{O_x, O_{in}, B_{in}\}$. The B_{in} configuration occurs for $K < K_{min}$ (then also $K \in \mathbf{K}_*$) or $K \in]K_{Max}, 1[$. At fixed $\ell \in \mathbf{L1}$, there can be the inner B_{in} in \mathbf{K}_* : i.e., increasing $K > 0$, there is the sequence $\{B_{in}, (B_{in}, C), C_x, O_{in}\}$. If the starting point is $\ell \in \mathbf{L0}$, then, increasing $K > 0$, there is the sequence $\mathcal{B}_K = \{B_{in}, O_{in}\}$. In other words, the specific angular momentum is low enough to not lead to the formation of an outer lobe, but it eventually

opens in O_{in} . The B_{ext} , associated to O_{ext} for high values of the specific angular momenta, has morphology similar to the B_{in} surface. The B configurations for $\ell \in \mathbf{L2}$, where the cusped surfaces O_x can appear, are classified as B_{in} , in fact the B_{ext} ones are separated by O_{ext} for each value of $\ell \in \mathbf{L3}$ and any K value—see Fig. 4 and Fig. 2.

For parameter $K \in \mathbf{K0} > K_{Max}$, there are B_{in} surfaces opening for $K \geq 1$ as $O_{in} \in]O_{in}^\gamma, O_x^\gamma[$ and, similarly to O_{in} with $\ell \in \mathbf{L1}$, and O_{in} with $\ell \in \mathbf{L0}$. The presence of a minimum point of the hydrostatic pressure always implies, in a Kerr black hole geometry, the presence also of a maximum pressure point. The inverse is not true, for example for $\ell \in \mathbf{L3}$, when there is only one family of non-critical open surfaces O_{ext} at $r > r_\gamma$.

We summarizing saying that for $K \in \mathbf{K1}$ there are open surfaces for any specific fluid angular momentum ℓ . The cusped open configurations O_x , closed on the **BH**, are associated to parameters $\ell \in \mathbf{L2} \cup K \in \mathbf{K1}$, where the limiting surface is

$$K \in \mathbf{K1} \quad O_x > O_x^\gamma \quad \ell \in \mathbf{L2} \quad r_J \in]r_x^\gamma = r_\gamma, r_{mbo}] \quad (28)$$

$$\partial_{|\ell|} r_J < 0 \quad \partial_K r_J < 0, \quad \lim_{\ell \rightarrow \ell_\gamma} O_x \approx O_x^\gamma. \quad (29)$$

However, we have

$$\lim_{K \rightarrow \infty} O_{ext} \approx O_{ext}^\ell \quad \text{while} \quad \lim_{\ell \rightarrow \ell_\gamma} O_{ext}^\ell \approx O_x^\gamma. \quad (30)$$

The open surfaces, of O_{in} class with $\ell \in \mathbf{L2}$ are limited by O_{in}^ℓ at equal ℓ . These are limited by the boundary surfaces with specific angular momentum ℓ_{mbo} and ℓ_{mso} . However, as clear from the Fig. 3, for x large enough, the funnels of hy -surfaces go far from the source and, independently by the magnitude $\ell_a/\ell_b = -1$, the two ℓ counterrotating funnels are getting closer.

On the other hand, for sufficiently high magnitude of the specific angular momenta, i.e. $\ell \in \mathbf{L3}$ and $K \in \cup K0$, there are maximum pressure points but not the minimum of the hydrostatic pressure. Consequently there are closed stable C or open O_{ext} topologies. The Paczyński-Wiita instability can occur only after a reduction of the specific angular momentum, when the disk center approaches the attractor. If the specific angular momentum decreases from the $\ell \in \mathbf{L3} \cup K \in K0$ to $\ell \in \mathbf{L1} \cup K \in K0$, then the unstable phase will necessarily correspond to an accretion. If the decrease of specific angular momentum occurs with an increase of K , then it can give rise to the open cusped O_x surface. The high values of the specific angular momentum, $\ell \in \mathbf{L3}$ or also $\ell \in \mathbf{L2}$, are associated to closed equilibrium configurations or open surfaces. If the disk stretches sufficiently, the pressure at the inner edge can reach the proper minimum value to be open. On the other hand if there is $\ell \in \mathbf{L3}$, then the elongation of the configurations and fluid angular momentum magnitude are too high causing the opening of a O_{ext} surface.

V. CONCLUDING REMARKS

We focused on the open, unstable solutions of Euler equations for **RADs**, aggregations of several tori of one-species

particle perfect fluid centered on the equatorial plane of a Kerr **SMBH**. These structures, have been variously associated with jet of proto-jet emission. This investigation then fits into the more broad discussion on the role and significance of open surfaces in relation to (matter) jets emission and collimation, as well as jet-accretion correlation—see also [8–11, 14, 15, 18].

The issue of the location of the inner edge of a single torus is a relevant aspect of the possible jet-accretion correlation, relating jet-emission to the inner part of the accretion disk—see for a discussion of the inner edge problem [37, 42–45]. Attempts to characterized narrow, relatively long matter funnels of jets, here considered as proto-jets configurations, are for example in [43, 46–53]. For updated investigations on jet emission, detection and jet-accretion disk correlation see for example [54–62] and also [63–69].

After introducing the model for the single torus orbiting of the **RAD**, in Sec. (II) we discussed the main features of the ringed accretion disks, and the emergence of the different instabilities for the systems. The problem to find the solutions of the Euler equations for the **RADs** has been reduced to the study of the critical points for an effective potential describing the orbiting fluids with proper boundary conditions; in this way we could estimate very precisely the diverse contributions of the background and the centrifugal forces on dynamics of the single torus as well as on the set of configurations in the **RAD** and the entire agglomeration. In Sec. (III B), we have deepened this aspect by taking advantage of system symmetries, considering a different parametrization for the effective potential function highlighting the symmetry of motion and background represented by Kerr axi-symmetric solution. Eventually we introduced different rotational parameters. This has allowed us to highlight the role of the dimensionless radius $R \equiv r/a$ and of the fluid specific angular momentum with respect to the black hole spin, the ratio $\ell/a \sin \theta$, pointed out also in [2], and the quantities $\mathcal{A}^\pm = \ell \pm a$.

The analysis has ultimately singled out the role of the limiting surfaces, the γ -surfaces and $h\gamma$ -surfaces, for the open

configurations. We proved there is a strict correlation between different γ -surfaces (geometric surfaces of the space-time structure) and the $h\gamma$ -surfaces having roles in the matter models. The $h\gamma$ -surfaces limit the fluid configuration, while the γ -surfaces constraint the fluid, at variation of ℓ . The limiting geometric surfaces, γ -surfaces, are related to the geometric properties of the Kerr spacetimes inherited by the solution of Eq. (7), associated to the specific angular momentum $\{\ell_{mso}^\pm, \ell_{mbo}^\pm, \ell_\gamma^\pm\}_{\pi/2}$. Given the significance from the phenomenological point of view of different instabilities which characterize the toroidal population in the **RAD**, it is clear that a study of these constraints (especially in relation to the central attractor) is important. The limiting hydrostatic surfaces, $h\gamma$ -surfaces, are associated with each hypersurface Σ_ℓ , of constant specific fluid angular momentum, whose topology and morphology changes with the variation of one of the two system rotational parameters ($\ell, a/M$). At $\Sigma_{a/M}$, the γ -surfaces are the limits of the $h\gamma$ -surfaces, approached by varying ℓ ; the $h\gamma$ -surfaces in turn limit the matter fluid surfaces.

The role of these surfaces in the **RADs**, their origins and the destabilizing effects on the system were briefly addressed, possible magnetic effects in a magnetized **RAD** contests are discussed in [31], while a more thorough discussion of the boundary conditions for the open solutions are postponed to future analysis. We expect these considerations can play an important part in the phenomenological aspects connected with X-ray emission in **SMBH-AGNs** and in the study of the possibility for a jet-accretion correlation.

ACKNOWLEDGMENTS

D. P. acknowledges support from the Junior GACR grant of the Czech Science Foundation No:16-03564Y. Z. S. acknowledges the Albert Einstein Centre for Gravitation and Astrophysics supported by grant No. 14-37086G.

-
- [1] Abramowicz M. A. & Fragile P.C. 2013, Living Rev. Relativity, 16, 1,
 - [2] Pugliese D. & Montani G. 2015, Phys. Rev. D, 91, 083011
 - [3] Pugliese, D. & Stuchlík, Z. 2015, APJS, 221, 2, 25
 - [4] Pugliese, D. & Stuchlík Z. 2016, APJS, 223, 2, 27
 - [5] Pugliese, D. & Stuchlík, Z. 2017, APJS, 229, 2, 40
 - [6] Pugliese D. & Stuchlík Z. 2018, JHEAp 17 1
 - [7] Paczynsky B. Wiita P. J. 1980, A&A 88, 1-2, 23-31
 - [8] Kozłowski, M., Jaroszyński, M. & Abramowicz, M. A. 1978, A&A 63, 1–2, 209–220.
 - [9] Sadowski, A., Lasota, J.P., Abramowicz, M.A. & Narayan, R. 2016, MNRAS, 456, 4, 3915
 - [10] Lasota, J.-P., Vieira, R.S.S., Sadowski, A., Narayan, R. & Abramowicz M. A. 2016, A&A., 587, A13
 - [11] Lyutikov, M. 2009, MNRAS, 396, 3, 1545–1552
 - [12] Blaschke M. & Stuchlík Z. 2016, Phys. Rev. D, 94, 8, 086006
 - [13] Stuchlík, Z., Blaschke, M., & Schee, J. 2017, Phys. Rev. D, 96, 104050
 - [14] Madau, P. 1988, Astrophys. J., 1, 327, 116-127
 - [15] Sikora, M. 1981, MNRAS, 196, 257
 - [16] Stuchlík Z., Slany P. and Hledlík S. 2000, Astron. Astrophys., 363, 425 9
 - [17] Slany S., Stuchlík Z. 2005, Classical and Quantum Gravity, 22 17
 - [18] Abramowicz, M.A., Jaroszyński, M. & Sikora, M. 1978, A&A, 63, 221
 - [19] Sochora, V., Karas, V., Svoboda, J. & Dovciak, M. 2011, MNRAS, 418, 276–283
 - [20] Karas, V. & Sochora, V., 2010, Astrophys. J., 725, 2, 1507–1515
 - [21] Schee, J. & Stuchlík, Z. 2009, Gen. Rel. Grav., 41, 1795
 - [22] Pugliese D., Quevedo H. & Ruffini R. 2011, Phys. Rev. D, 84, 044030
 - [23] Pugliese D., Quevedo, H. & Ruffini, R. 2013, Phys. Rev. D, 88, 2, 024042
 - [24] Pugliese D., Quevedo H. and Ruffini R. 2017, Eur. Phys. J. C 77, 4, 206
 - [25] Pugliese D., Quevedo H. and Ruffini R. 2011, Phys. Rev. D 83, 104052

- [26] Stuchlik Z., Slany P., Torok G. and Abramowicz M. A. 2005, *Phys. Rev. D* 71, 024037
- [27] Bicak J., Stuchlik Z., Balek V. 1989, *Astronomical Institutes of Czechoslovakia, Bulletin* 40, 2 65-92
- [28] Pugliese, D. & Quevedo, H. 2015, *Eur. Phys. J. C*, 75, 5, 234
- [29] Pugliese, D. & Kroon, J.A.V. 2012, *Gen. Rel. Grav.*, 44, 2785
- [30] Zanotti, O. & Pugliese, D. 2015, *Gen. Rel. Grav.*, 47, 4, 44
- [31] Pugliese D. & Montani G. 2018, arXiv:1802.07505 [astro-ph.HE].
- [32] Lei, Q., Abramowicz, M. A., Fragile, P. C., Horak, J., Machida, M. & Straub O. 2008, *A&A*, 498, 471
- [33] Witzany V. & Jefremov P. 2017, arXiv:1711.09241 [astro-ph.HE].
- [34] Abramowicz, M. A. 2008, arXiv:astro-ph/0812.3924
- [35] Boyer, R.H. 1965, *Proc. Camb. Phil. Soc.*, 61, 527
- [36] Abramowicz, M. A. 1971, *Acta. Astron.*, 21, 81
- [37] Paczyński, B. 2000, astro-ph/0004129.
- [38] Bejger M., Piran T., Abramowicz M. and Hakanson F. 2012, *Phys. Rev. Lett.*, 109, 121101
- [39] Ried K., Megan A., Vermeyden L., Janzing D., Spekkens R. W. & Resch K. J. 2015, *Nature Physics* 11, 414–420
- [40] Poisson E., *A Relativist's Toolkit: The Mathematics of Black-Hole Mechanics*, Cambridge University Press, (2004).
- [41] Pugliese D. & Quevedo H. 2018, *Eur. Phys. J. C* 78, 1, 69
- [42] Krolik, J.H. & Hawley, J.F. 2002, *Astrophys. J.*, 573, 754
- [43] Bromley, B. C., Miller, W. A. & Pariev, V. I. 1998, *Nature (London)*, 391, 54, 756
- [44] Abramowicz, M.A., Jaroszynski, M., Kato, S., et al. 2010, *A&A*, 521, A15
- [45] Agol, E. & Krolik, J. 2000, *Astrophys. J.*, 528, 161
- [46] Marscher, A. P., Jorstad, S. G., Gomez, J. L., et al 2002, *Nature (London)*, 417, 625–627
- [47] Maraschi, L. & Tavecchio, F. 2003, *Astrophys. J.*, 593, 667
- [48] Chen, Y., Zhang, X., Zhang, H. et al 2015, *apss*, 357, 2, 100
- [49] Yu, X., Zhang, X., Zhang, H., Xiong, D., et a. 2015, *Ap&SS*, 357, 14
- [50] Zhang J., Xue Z.W., He J.J., Liang E.W. & Zhang S.N. 2015, *Astrophys. J.*, 807, 1, 51
- [51] Sbarrato, T., Padovani, P. & Ghisellini, G. 2014, *MNRAS*, 445, 1, 81.
- [52] Maitra, D., Markoff, S., Brocksopp C., et al. 2009, *MNRAS*, 398, 4, 1638–1650
- [53] Ghisellini, G., Tavecchio, F., Maraschi, L., et al. 2014 *Nature (London)*, 515, 376
- [54] Liska M., Hesp H., Tchekhovskoy A., Ingram A., van der Klis M., Markoff S. 2018., *MNRAS: Letters*, 474
- [55] Caproni A., Abraham Z., Motter J. C. and Monteiro H. 2017, *Astrophys. J.*, 851, 2, L39
- [56] Inoue Y., Doi A., Tanaka Y. T., Sikora M. and Madejski G. M. 2017, *Astrophys. J.* 840, 1, 46
- [57] Gandhi P. *et al.* 2017, *Nature Astronomy*, 1, 864
- [58] Duran R. B., Tchekhovskoy A. and Giannios D. 2017, *MNRAS*, 469, 4, 4957
- [59] Vedantham H. K. *et al.* 2017, *Astrophys. J.* 845 2, 89
- [60] Bogdsn A., Kraft R. P., Evans D. A., Andrade-Santos F. and Forman W. R. 2017, *Astrophys. J.* 848, 1, 61
- [61] Banados E. *et al.* 2018, *Nature*, 553, 7689 473
- [62] D'Ammando F. 2017, *Front. Astron. Space Sci.* 4, 53
- [63] Neilsen J. & Lee J. C. 2009, *Nature* 458, 481–484
- [64] Fender R. P. 2010, *Lect. Notes Phys.* 794, 115
- [65] Fender R. & Belloni T. 2004, *Ann. Rev. Astron. Astrophys.* 42, 317
- [66] Soleri P. *et al.* 2010, *MNRAS*, 406, 1471
- [67] Tetarenko B. E., Lasota J.-P., Heinke C. O., Dubus G. & Sivakoff G. R. 2018, *Nature*, 554, 69–72
- [68] Toba, Y., Komugi, S., Nagao, T., et al. 2017, *Astrophys. J.*, 851, 98
- [69] Fang K. & Murase K. 2018, *Nature Physics*, Letter doi:10.1038/s41567-017-0025-4